Development of a general formalism to analyze plasmonic structures using spectroscopic ellipsometry

R. Verre,[*,†] M. Modreanu,[‡] O. Ualibek,[,†] D. Fox,[,†] K. Fleischer,[,†] C. Smith,[,†] H. Zhang,[,†] M. Pemble,[,‡] J. F. McGilp,[,†] and I. V. Shvets[,†]

Centre for Research on Adaptive Nanostructures and Nanodevices (CRANN) and School of Physics, Trinity College Dublin, Dublin 2 , Ireland, and Tyndall Institute, Unversity of Cork, IRELAND

E-mail: rverre@tcd.ie

Abstract

Spectroscopic ellipsometry (SE) has been used to measure the full optical response of plasmonic structures. Firstly, the simple case of an anisotropic thin plasmonic layer supported on a transparent substrate is analysed by introducing a quantity named anisotropic surface excess function (ASEF). Such a quantity can be directly extracted from the experiment and simulated using either analytical or numerical methods. Afterwards, the formalism has been generalised using a transfer matrix method. In this way effects on the ellipsometric spectra of thick plasmonic films, anisotropic substrates, plasmonic structures grown on top of a multilayer system are described in terms of

[*]To whom correspondence should be addressed

[†]Centre for Research on Adaptive Nanostructures and Nanodevices (CRANN) and School of Physics, Trinity College Dublin, Dublin 2 , Ireland

[‡]Tyndall Institute, Unversity of Cork, IRELAND

changes in the effective dielectric function of the system. The analysis developed here has been supported by experimental evidences obtained by measuring the response of anisotropic NP arrays grown at glancing angle. The agreement between theory and experiment is clear, suggesting that SE can be conveniently employed to measure the spectroscopic response of plasmonic structures. It is also demonstrated how the figure of merit of the plasmonic resonances can be greatly improved, with particular measurement configurations, using SE. This can increase the sensitivity of any refractive index based plasmonic sensor. Finally, compared to normal transmission spectroscopies, SE can easily measure the out-of-plane response of the plasmonic systems, providing a much more stringent test for the suitability of certain models to simulate the far field response of a plasmonic system.

Introduction

The interaction between electromagnetic waves and free electrons in a low-dimensional metallic structure results in surface plasmon effects.[1,2] These can be considered as the normal excitation modes of the systems and have been the subject of tremendous interest due to their application as biological sensor,[3–6] enhancement effects[7–9] and solar cell applications.[10–12] When a metal nanoparticle (NP) is excited the electrons are highly localised and decay rapidly within the structures, resulting in localised plasmon resonances (LPRs).

LPRs manifest themselves readily by strong absorption/reflection peaks whose positions depend on the shape, size and aspect ratio of the NPs, on the property of the surrounding medium and on the relative interaction between the NPs.[13] Their behaviour is usually analysed using conventional spectroscopic methods in the far field, but recently their charge distribution has been also addressed using more specific characterisation methods such as cathodoluminescence,[14,15] transmission electron microscopy[16] and electron energy loss spectroscopy.[17] The main limitation of conventional absorption spectroscopies is it allows one to monitor only in-plane properties of the plasmonic structures due to the inherited difficulties

in the measurement geometry. To overcome this problem Spectroscopic Ellipsometry (SE) can be utilised as it can analyse changes in the polarization state of a linearly polarized beam reflected at oblique angles of incidence.[18,19] Recently, SE analysis has been extended to magnetic[20] or anistropic samples[21] using generalised ellipsometry. Scattering and depolarization properties of the samples can also be addressed and separated by normal specular reflection. However, SE spectra are difficult to analyse as the response of the whole system needs to be modelled and compared with experiment to address the properties of the samples investigated.[18] For this reason, the number of studies of plasmonic structures using SE is still limited.[22–26] Previously it was demonstrated by our group[27] that a quantity, named Anisotropic Surface Excess Function (ASEF), could be extracted from the experiment and the response of ultrathin plasmonic layer (<10 nm) directly analysed. The great advantage of ASEF is it depends only on the optical properties of the plasmonic layer alone, rendering easy the modelling of the nanocomposite layer alone.[27,28] However, the hypothesis for the validity of this approach appears to be limited to very specific cases.

At the same time many theories have been developed to describe the optical properties of plasmonic structures. The first attempt dates back to the beginning of the last century, when Mie calculated the absorption cross section of spherical NPs in a host matrix based on the development of electromagnetic potentials in spherical harmonics.[1] For a metallic sphere, with dimensions much smaller than the exciting light, the polarization of the NP leads to a simple dipole behaviour placed at the centre of the sphere. However, this behaviour can be strongly modified. For example, the elongation of a sphere along certain directions lowers the symmetry of the system, resulting in the formation of multiple resonance peaks, corresponding to the different excitation modes of NP. Interaction with a substrate produces image charge effects that modify the optical response of the system. The work by Yamaguchi[29,30] qualitatively reproduced the experiment. However, as recently pointed out,[31] more refined theories are required to quantitatively model the experimental behaviour. Also electromagnetic interactions between closely spaced NPs produce a shift in the resonance

position and, for particular NP arrangements, Fano modes are also found which result in sharp resonances.[5,32–35] More complicated phenomena arise when irregularly shaped NPs are simulated. In this case many different charge excitation patterns can be formed due to changes in the susceptibility of the NP itself.[36] Only numerical methods, such as finite element methods,[37,38] finite-difference time-domain[39] or discrete dipole approximation[40,41] can reproduce the behaviour of such systems. Depending on the system analysed a suitable model then needs to be applied and compared with experiment. SE can be utilised within this framework to test the validity of the approach chosen. Furthermore, as the out-of-plane resonances are also measured, they can no longer be treated as a free parameter and a modelling of the full optical response of the system is required.

In this article a detailed study of LPRs with SE will be performed. The plasmonic layer will be produced using an alternative self-assembled method based on glancing angle of incidence on a stepped template.[42–45] Adatoms are sent at shallow angles of just a few degrees onto a faceted c-plane Al_2O_3 and part of the surface is shadowed by the presence of the steps. Adatoms are only deposited in the exposed areas and spontaneously rearrange into NP arrays (see Figure 1). The technique is simple and large homogeneous areas covering the entire

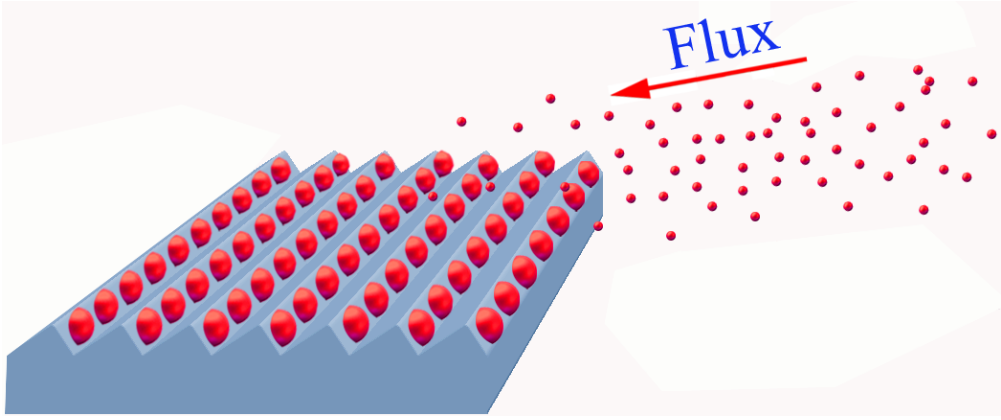

Figure 1: A schematic view of the deposition technique: a flux of collimated adatoms is sent towards the surface at a glancing angle of incidence and coalesces on the step of a patterned surface, forming NP arrays.

surface are realised. Furthermore, the technique has been shown to be largely independent of the deposited metal type as NP arrays of different materials have been produced using

this method.[46] During the manuscript the capabilities of extracting the plasmonic response of the system using the ASEF approach will be tested on the samples grown and then reproduced with a dipolar method previously developed.[47] This will provide a basis for the understanding of the various spectra measured. Afterwards, a more general formalism will be introduced and effects which induce changes in the optical properties in the whole will be systematically analysed. It will be also be demonstrated the striking advantage of using SE when compared with simple absorption spectroscopy in monitoring changes in the refractive index of the medium surrounding the probed NPs. Sharper resonances can be measured and increases in the figure of merit (FOM) of the resonance up to 15 times have been measured. This could improve the detection limit of refractive index based sensors. This study will open new exciting possibilities in the analysis of the plasmonic response of structures using spectroscopic ellipsometry.

ASEF and plasmonic modelling

In general, an analytical expression representing the properties of a single layer cannot be directly extracted from SE experiment. Multiple internal reflections modify the final expression of the pseudo-dielectric function $< \varepsilon_j >$ of the system considered as a whole homogeneous medium. A simple additivity of each layer hence does not hold any more. The case of plasmonic nanostructure is even more complicated, as the layer is not homogeneous. However, if the dimension of the structures involved (roughness and NP dimensions) are much smaller than the wavelength of the exciting light, the nanocomposite layer can be treated as a continuous and homogeneous layer with an effective dielectric function ε_L which in turn can be anisotropic.

In a three phase approach (substrate, plasmonic layer and air), if the nanocomposite layer is thin, the substrate response is isotropic and the optical axes are aligned with the symmetry axis of the system, the picture can be incredibly simplified. In this case, the

additivity between the response of each layer can be assumed to hold to the first order and the ASEF can be extracted directly from the experiment as[28,48,49]

$$\xi_j = \frac{i\lambda(\varepsilon_b - 1)}{4\pi\varepsilon_b\sqrt{\varepsilon_b - \sin^2\Theta}}(<\varepsilon_j> - \varepsilon_b). \tag{1}$$

In Eq. (1) λ is the vacuum wavelength in nm, Θ is the angle of incidence, ε_b is the substrate dielectric function and air is considered as the surrounding medium.

Usually, ellipsometric observables are expressed in terms of the complex ratio ρ. However, the psuedo-(effective) dielectric function for the whole bulk system appearing in Eq. (1) can be extracted from the raw measurements by

$$<\varepsilon> = \sin^2\Theta + \sin^2\Theta\tan^2\Theta(\frac{1-\rho}{1+\rho})^2. \tag{2}$$

Once the substrate dielectric function is known, ASEF can hence be extracted directly from the experiment using Eq. (1).

The advantage of introducing the ASEF relies on its simplicity as it depends on the response of the (anisotropic) plasmonic layer alone, which can then be modelled by[28]

$$\xi_j = d[(\Delta\varepsilon_j + \varepsilon_b\Delta\frac{1}{\varepsilon_z}) + (\frac{1}{\varepsilon_b} - \frac{\cos^2\Theta}{\sin^2\Theta})(\Delta\varepsilon_j - \Delta\varepsilon_k)]. \tag{3}$$

where $j,k = (x,y)$. The coefficients in Eq. (3) are defined by

$$\Delta\varepsilon_j = \varepsilon_{L,j} - \varepsilon_b \qquad \Delta\frac{1}{\varepsilon_z} = \frac{1}{\varepsilon_{L,z}} - \frac{1}{\varepsilon_b} \tag{4}$$

and d is the effective thickness of the homogeneous NP layer. The nanocomposite response can then be extracted by Eq. (1) and any suitable model capable of calculating the dielectric function of the plasmonic layer can be directly compared with the experiment using Eq. (3). The problem of analysing the response of the whole system has been reduced in this case to

the determination of the plasmonic layer dielectric function.

To compare the theory with experiment, the system investigated in this manuscript has been modelled as collection of supported identical ellipsoids placed on a rectangular lattice interacting through dipolar forces. Due to the small dimensions involved, the quasistatic approximation is assumed to be valid. Under this hypothesis an expression for ε_L reads as[27,47]

$$\begin{aligned} \varepsilon_{L,i} &= \varepsilon_{cap}(1+\frac{N\alpha_i}{1+\alpha_i\beta_i}) \qquad i=x,y \\ \frac{1}{\varepsilon_{L,z}} &= \frac{1}{\varepsilon_{cap}}(1-\frac{N\alpha_z}{1+\alpha_z\beta_z}) \end{aligned} \tag{5}$$

where ε_{cap} is the homogeneous dielectric function of the capping material, N is the number of NPs per unit area and α is the polarizability of an isolated ellipsoid. The β coefficient represents the interaction effects and takes into account both NP interactions and image charge effects. In order to take into account the effect of the steps, the capping medium dielectric function has been considered as a mixture between air and substrate in a 1:1 ratio.[47] In the rest of this manuscript the in-plane directions will be referred as x (along the NP rows) and y (perpendicular to the rows), while the out-of.plane direction will be defined as z (see Sketch in Figure 3). Using Eq. (3) and Eq. (5) the ASEF of the plasmonic layer can then be modelled and directly compared with experiment. In the next section it will be demonstrated the utility of the ASEF approach to model and understand the full optical response of the whole system.

Results and discussion

The SEM of the in-plane structure deposited at glancing angle is shown in Figure 2 A. The structure appears as a collection of ordered NP arrays aligned along the step edges as previously reported. The in-plane semi-axes ($R_x = 12\,\text{nm}$ and $R_y = 10\,\text{nm}$) are well below

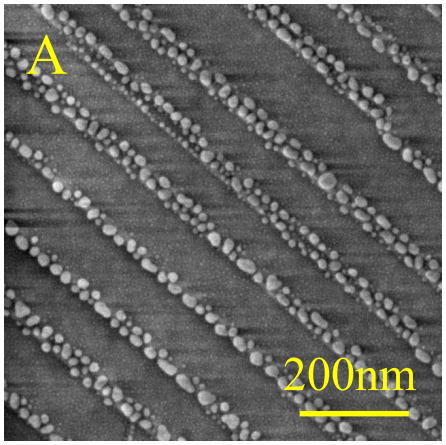

Figure 2: (A) Scanning electron micrograph of the Ag NP arrays deposited at a glancing angle of 6°. Rows of NP arrays are clearly visible along the step edge of the stepped template. Low magnification and high magnification transmission electron microscope (TEM) of a section of the same samples are shown in B and C respectively.

the diffraction limit and the plasmonic layer can therefore be considered as an homogeneous anisotropic layer. As the centre-to-centre distance L_x, is 27 nm the inter-particle separation ($\sim$3 nm) is much smaller than the average NP diameter, a strong enhancement of the electric field is expected to take place in the interstitial space between NPs. In order to fully characterize the sample, the out-of-plane morphology has been also analysed by TEM (see Figure 2 B and C (NOT YET PRESENT)), revealing the NPs appear as truncated ellipsoids of height $H = 17$ nm. Details of the exact growth mechanism of such structures can be found elsewhere.[47]

The response of the structures grown have been first analysed by SE using the same angle of incidence $\Theta = 61°$, and by changing the azimuth of the sample in the plane of incidence by an angle φ (Figure 3). This incidence angle was first chosen as it close to the Brewster angle of the Al_2O_3 substrate in the visible region. In this case, as discussed in our earlier paper on the plasmonic response of similar structures,[27] the ratio between the p and s components is maximised and the measurements are simplified. The measured azimuthal real and imaginary response of the structure are shown in Figure 3 A and B respectively. Superimposed onto the substrate behaviour additional features are clearly visible. The ASEF extracted from the experiment using Eq. (1) and modelled by Eq. (3) and Eq. (5) are shown in Figure 3

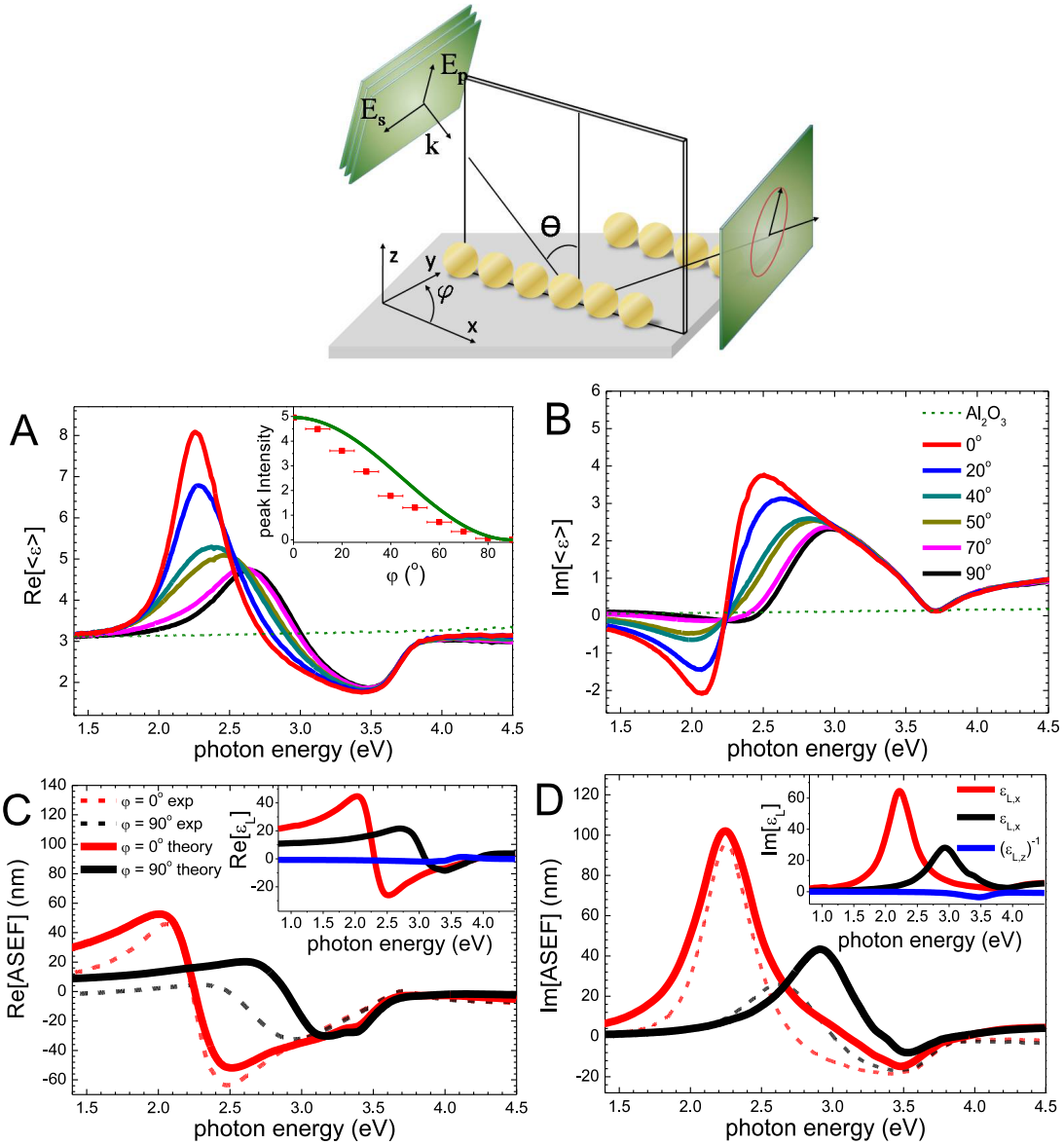

Figure 3: Real (A) and imaginary (B) parts of the pseudo-dielectric function $< \varepsilon >$ of Ag NP arrays grown at glancing angle for different azimuthal angle rotations φ. The intensity of the x resonance at 2.2 eV follows a $\cos^2$ dependency (inset in Fig. A). Both experimental (dotted lines) and simulated (continuous) ASEF for the parallel ($\varphi = 0°$) and perpendicular ($\varphi = 90°$) measurement configurations are also shown (C and D). An analysis of the ASEF suggests that the peaks observed in the real part of the pseudo-dielectric functions are related to the resonances of the plamsonic layer (see the imaginary part of ε_L in the inset).

C and D. A semi-quantitative agreement is clearly observable. The slight disagreement in the position of the y resonance could be explained by sample disorder. In the real system, double chains can be sometimes be observed and they can influence the peak position of the plasmonic response, shifting the y resonance towards the IR. Also, as the truncated NPs are modelled as ellipsoids supported on the substrate, mismatch between theory and experiment can be expected. The disagreement observed is then related to limitations in the model utilised rather than incorrect analysis of the results. However, we want to stress here that no fitting parameter has been introduced in the simulation and that the simulated spectra are obtained using only morphological parameters measured by micrographic analysis.

From Figure 3 A, for the measurement configuration parallel to the array ($\varphi = 0°$), a positive peak can be observed at $\sim$2.2 eV, together with a minima present at higher energies. As previously discussed[27] and suggested by the theory (see the dielectric function of the layer in the inset of Figure 3 C and D) the positive feature in the imaginary part of the ASEF is related to resonances along the x direction , while the minima at higher energy corresponds to the z resonance. The opposite sign in the out-of-plane z resonance is due to the discontinuity of the perpendicular component of the electric field in Maxwell Bounduary conditions.[29] By rotating the sample towards the measurement configuration perpendicular to the array ($\varphi = 90°$) the intensity of the 2.2 eV decreases monotonically following a $\sim \cos^2(\varphi)$ dependency (see inset in Figure 2 A). The behaviour can be explained by rotating the sample symmetry axis along the optical axis. In this case the rotation of the layer dielectric tensor in Eq. (5) can be expressed by the matrix

$$A(\varphi) = \begin{pmatrix} \cos\varphi & -\sin\varphi & 0 \\ \sin\varphi & \cos\varphi & 0 \\ 0 & 0 & 1 \end{pmatrix}. \tag{6}$$

Defining now A^T as the transpose of A and remembering that the dielectric tensor of the plasmonic layer upon in-plane rotation can be expressed as $A^T \varepsilon_L A$, the $\cos^2$ behaviour for

the x resonance measured is reproduced.

It is important at this point to note that, comparing the normal bulk values, for thin plasmonic films and transparent substrates as the one here analysed, the absorptive component of the plasmonic layer is present in the real part of the pseudo-dielectric function. This reversal between $Re[<\varepsilon>]$ and $Im[\varepsilon_L]$ can be easily explained by the imaginary term i present in Eq. (1). We want to stress that the validity of the ASEF approach here utilised is constrained to a ultra-thin plasmonic layers and isotropic bulk responses.[28] However, under these assumptions, a direct comparison between theory and experiment can be directly achieved by assessing the response of the anisotropic thin plasmonic layer along the sample anisotropic main axis (φ=0° and 90°) at the substrate Brewster angle. In this way it is possible to minimize mixing between p and s components of the reflection coefficients (hence mixing of the response of both x and y resonances) and the resonances can be immediately attributed to the in-plane and out-of-plane resonances along the symmetry directions of the system. Clearly, the measurement for isotropic samples are further simplified as the dependency on the azimuthal rotation angle is removed.

Extension to a more general formalism

In the previous section it was shown that the ASEF approach can be successfully applied to the analysis of ultrathin plasmonic layers. It was also shown that the simulation reproduced the results even when the optical axis were not aligned with the principal axis of the system, provided an opportune rotation of the dielectric tensor was performed. However, the validity of the ASEF approach is severely constrained to very specific cases. For example, for multilayer structures or thick plasmonic layers, the formalism previously introduced is no longer accurate.

In this section a more general formalism, based on a transfer matrix approach developed by Schubert is applied.[50,51] Following his approach, an analytical expression for the

transmission matrix of the whole system can be obtained and the complex Fresnel reflection coefficient for p and s polarized light derived. The reflection ratio $\rho = r_p/r_s$ can then be calculated, an expression for the pseudo dielectric function obtained using Eq. (2) and compared with experiment. The only input parameters required for the application of this method are the dielectric function of each layer and the respective thickness. Any method which allows one to model the dielectric function of the plasmonic layer can then be compared directly with the response measured by SE. For example, if absorption spectra are obtained from some numerical simulation, one could calculate the imaginary part of the dielectric function of the plasmonic layer through the optical theorem[52] and extract the real part through the Kremers-Kronig relationship. In the following the effect of different factors on the spectra as measured by SE will be discussed and a direct comparison with experiment whenever possible.

The validity of the approach has been first verified for parallel and perpendicular configuration by comparing the simulations with the Ag spectra measured at different angles of incidence. The resonances appear in the real part of the pseudo dielectric function, so the real component only for the configurations parallel and perpendicular to the arrays are reported here. From Figure 4 a strong agreement between experiment and theory can be noticed and a similar one was observed also for the imaginary component. First, one can notice that the pseudo-dielectric function of the whole system depends heavily on the angle of incidence as the optical path in changed. As the sample is anisotropic, the reflection is different along the two orthogonal in-plane directions. In this case, by varying the angle of incidence, different p and s components are probed, resulting in a strong change in the reflection ratio (and hence in the pseudo dielectric function). For the perpendicular configuration (Figure 4 B and D), one can observe that the y resonance peak shift is correctly reproduced for various angle of incidence but the changes in intensity are not. The disagreement is as before due to a shift between the simulated y resonance and the measured one, rather than an incorrect analysis of the SE results.

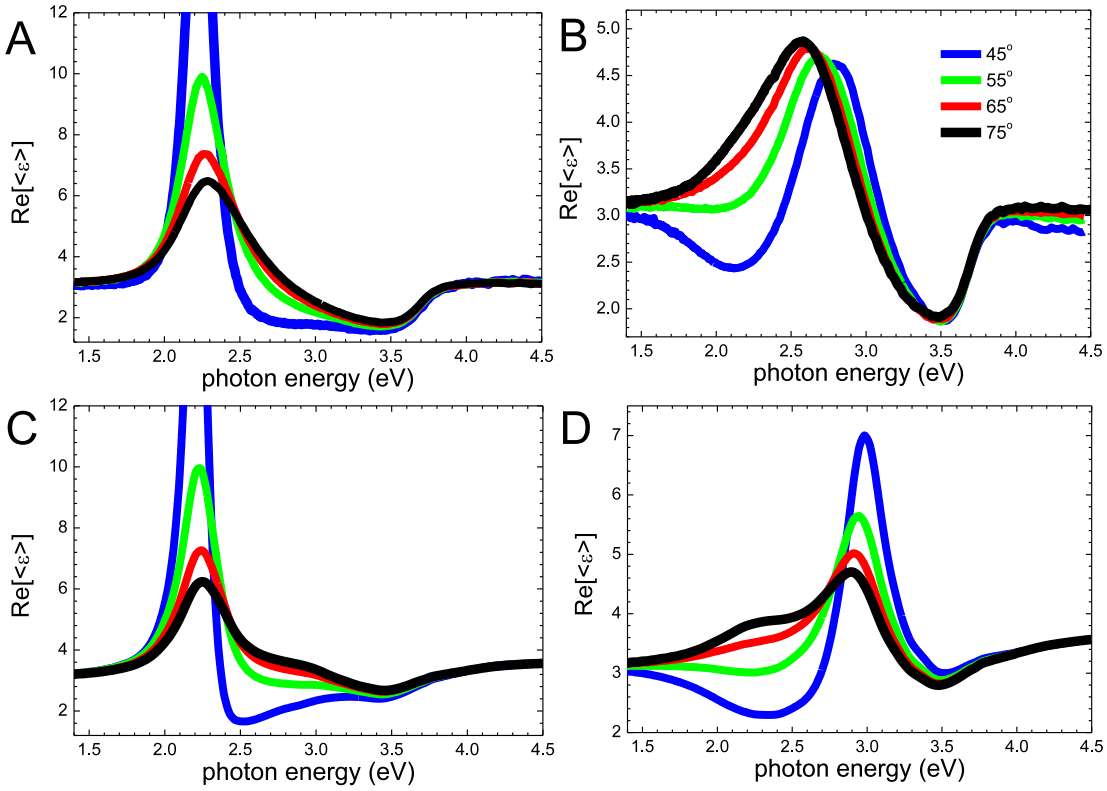

Figure 4: Real part of the pseudo-dielectric function for the measurement configuration parallel (A) and perpendicular (B) to the array at different angles of incidence. The simulated pseudo-dielectric functions for the two cases calculated using the transfer matrix formalism are shown in (C) and (D) respectively. The x resonance peak at $\sim$2.2 eV observed in (A) and (C) for 45° angle of incidence has an intensity of $\sim$16.

Of particular interest is the fact that for $\varphi = 0^\circ$ measurement configuration (Figure 4 C) the intensity of the positive peak at 2.2 eV increases by a factor of 3 when going from $\Theta = 61^\circ$ to closer $\Theta = 45^\circ$ and at the same time the resonance shows an even sharper peak. This effect is well reproduced by the simulation. The strong increase in the resonance profile is related to the presence of a singularity in the imaginary part of r_s whenever the angle of incidence is close to $\Theta \sim 35^\circ$. In case of anisotropic samples, the possibility of measuring such sharp resonances could be of great interest as the figure of merit (FOM) of the sharp resonance structure is greatly increased in this case. In particular, for $\Theta = 45^\circ$ an increase of the FOM by factor $\sim$15 if compared with $\Theta = 70^\circ$ incidence angle has been realised. For this particular system, the simulations suggest that the FOM can be even further increased if the measurement angle is closer to the singularity for r_s at $\Theta \sim 35^\circ$. These results suggest that the sensitivity of any refractive index plasmon-based biosensor can be theoretically increased by choosing the appropriate incidence parameters during a SE measurements.

As a representative example, in Figure 5 a comparison is shown between the simulated absorption and SE spectra when the NP arrays are surrounded by different dielectric media. During the simulations the absorption profiles were obtained using the relation $A_{\mathrm{abs},x} \propto \mathrm{Im}[\varepsilon_{L,x}]/\lambda$.[52] As expected, an increase in the refractive index surrounding the NPs red shifts in the x resonances position. However, a much sharper profile is obtained for the pseudo-dielectric function. This result potentially opens a new route for sensing applications using SE. Furthermore, as SE is based on measurements of only relative changes in the dielectric function of the medium, a larger accuracy can be achieved if compared with standard transmission measurements. Similar enhancement have been recently reported for in-plane symmetric system once the phase of the complex ratio ρ is measured.[25]

The transfer formalism developed by Schubert can be also adapted to other optical characterization method and different materials (see supporting information for reflectance anisotropy spectroscopy measurements and SE measurements on Au NP arrays). Also, the theory presented here could be extended to magnetically active systems and core-shell struc-

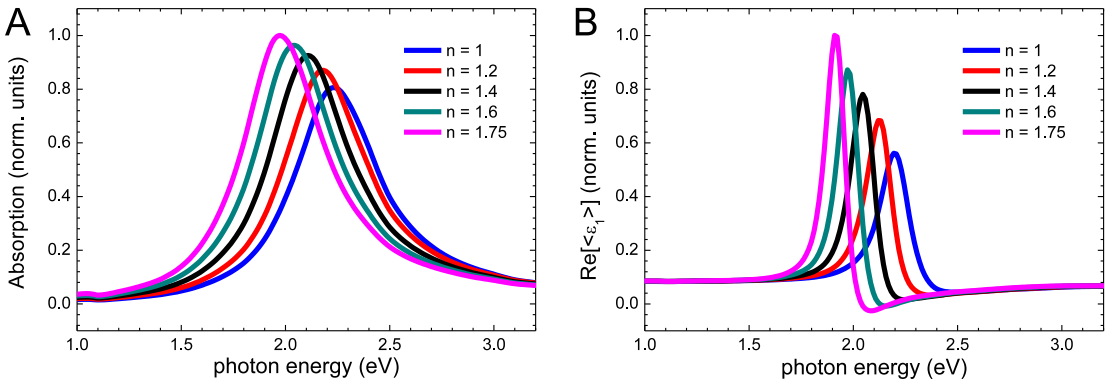

Figure 5: Simulation of the absorption along the NP arrays (A) and of the pseudo-dielectric function (B) in the parallel configuration at 45° the NP array system upon changes of the dielectric medium covering the particles. Red shift in the x resonance can be observed for increasing the dielectric medium. However, the FOM simulated using SE can be greatly increased when compared with normal absorption spectroscopy.

tures.[51,53]

Based on the results reported so far, we believed that the transfer matrix approach here proposed is a suitable and convenient method to simulate and analyse the spectroscopic response of plasmonic structures. In the following possible additional effects which could influence the response of the system are discussed using the simulation developed. Figure 6 and Figure 7 show the SE spectra for the different cases of increasing layer thickness and different substrates (Si rather than Al_2O_3) respectively. In order to facilitate the analysis, during these simulations the plasmonic layer was assumed to be in-plane isotropic ($R_x = R_y = 20\,\text{nm}$ and $R_z = 7.5\,\text{nm}$) and with particles spacing large enough to disregard any inter-particle coupling ($N = 7 \times 10^{13}\,\text{NP/m}^2$). The self-image charge contribution produced by a the presence of a thin Al_2O_3 layer underneath the NPs is still taken into account. With these parameters, the dielectric function of the layer for the two examples is shown in Figure 6 A. As the sample is in-plane isotropic, $<\varepsilon>$ is now independent either on the azimuthal rotation angle φ and on the angle of incidence Θ. However, it can be easily seen in that changes in the plasmonic films film thickness result in a strong modification of the SE response. As previously discussed when an ASEF was introduced, for an ultra-thin structure the maximum in $\text{Re}[<\varepsilon>] \propto \text{Im}[\varepsilon_L]$. The relation is valid whenever the plasmonic film d is

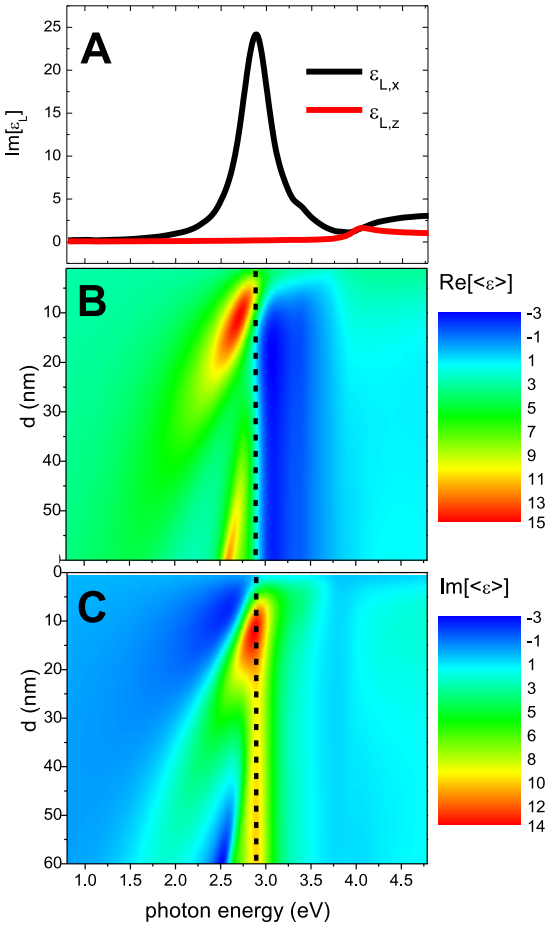

Figure 6: (A) Simulated imaginary part of the dielectric function of supported isotropic spheroids along the x and z direction. The contour plot of the real and imaginary part of the calculated psuedo-dielectric function for different plasmonic layer thickness d are shown in B and C respectively. The vertical dotted line shows the position of the x resonance and it is used as a guideline.

thin, i.e.

$$d \ll \frac{\lambda}{4\pi\sqrt{\varepsilon_{L,j} - \sin^2\theta}}. \tag{7}$$

Figure 6 now allows to a more precisely quantification of Eq. (7):even for an effective plasmonic layer of 5 nm a mixture between the real and imaginary component takes place and the ASEF approximation is no longer valid. Larger layer thickness results in a complex behaviour which can hardly relate directly to the plasmonic features but it can be addressed using our transfer matrix approach. Modifications also take place when a non transparent substrate is used. For example, in the case of Si substrates, it is shown that the plasmonic features of ultrathin films are hardly visible as the substrate is strongly dispersive. Furthermore, the overall signal lowers when larger film thicknesses are modelled. The opposite trend is expected for transparent non dispersive substrates such as Al_2O_3.

The results shown suggest that the SE response originated by plasmonic structures depends on many contributing factors, such as NP morphologies, material compositions and substrate dielectric function and the overall response can be heavily modified by changes in any of them. However, the unknown parameters can be treated as fitting parameters and the modelling achieved using self-consistent methods. Similar to standard ellipsometric results of multilayer structures, an initial guess of the pseudo-dielectric function can be introduced and compared with the experimental results. Then by varying the unknown parameters a match with experiment can be obtained. In this case, clearly, analytical simulations such as the one here introduced are much more suited for fast convergence.

Conclusions

In conclusion, we have demonstrated and developed a methodology to investigate the plasmonic response of complex NP material systems. All the simulations were directly compared with experiment performed by measuring the spectral response of anisotropic NP arrays grown at glancing angles. First, a quantity named Anisotropic surface Excess Function

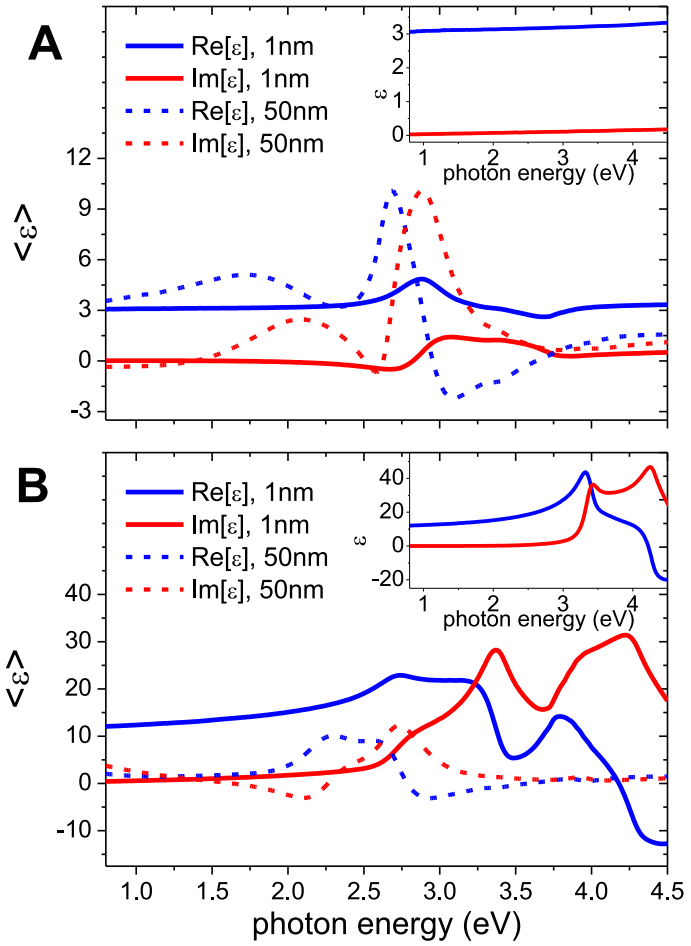

Figure 7: Pseudo dielectric function of isotropic spheroids supported on substrates Al_2O_3 (A) and Si (B) substrates for different plasmonic thickness. In the inset the bare substrate dielectric function in the two cases are shown.

(ASEF) is introduced and it is demonstrated how the plasmonic response of layer can be directly observed.

Afterwards, the formalism is further developed utilising a transfer matrix method. Different effects which can lead to a modification in the response of the system are discussed and a clear route for a complete analysis outlined. The approach can be adapted to thick NP layers, anisotropic systems, magnetically active systems, core-shell structures and different classes of material.

The results here show striking advantages. First, as SE can easily measure both the in-plane and out-of-plane response, this technique provides a more stringent test for the validity of any simulation method. Second, it is demonstrated here that in the case of anisotropic layers the resonance FOM can be greatly increased at a particular angle of incidence. In this way the sensitivity of any biological sensor based on the detection of changes of the dielectric medium surrounding the plasmonic NPs can be incredibly improved.

Methods

Noble metals NP arrays have been produced by glancing angle deposition on a single crystal c-plane Al_2O_3 templates. The substrates were off-cut 6° along the $[1\bar{2}10]$ direction and polished on one side. To produce the stepped surfaces[54,55] two samples were annealed at 1400°C in atmosphere for 16 h. AFM analysis confirmed the texturing of the template with a measured periodicity $L_y = 130\,\text{nm}$. Each sample was then loaded in a ultra high vacuum chamber (base pressure 2×10^{-8} mBar) and either Ag or Au was deposited at 6° with respect to the normal. During the deposition a calibrated rate at normal incidence of 2.5nm/min was utilised and the samples were exposed for 20 minutes. The deposition was performed at room temperature.

The in-plane morphology was imaged by a field emission ULTRA scanning electron microscope (SEM) by Carl Zeiss. SE measurements were recorded with a Woollam M2000

varible angle spectroscopic ellipsometry system, equipped with a rotating compensator and a high speed CCD camera. The measurements were performed between 245-1600 nm taking 670 points. The sample was aligned at each angle of incidence and rotated manually around the surface normal. The estimated error in the accuracy of the rotation angle was established to be $\pm 5^{\circ}$.

After measurements, Ag NP sample was capped with a 50 nm Si_3N_4 layer. The deposition was performed using a Plasma Enhanced chemical vapour deposition using 5% SiH_4 and NH_3 as precursors (1:6 ratio). During the process a growth temperature of 300°C was utilised using an RF frequency of 187.5 kHz for a total growth time of 6.15 minutes.

In order to analyse the out-of-plane morphology of the Ag capped sample, TEM out-of-plane sections were prepared using a Carl Zeiss Auriga CrossBeam FIB-SEM as already described before. Once prepared, the section was imaged by a Titan TEM operating at 300 kV. The substrate was aligned to the $[10\bar{1}0]$ zone axis for imaging. In all cases the images were acquired in bright-field mode.

Acknowledgement

This work has been funded by Science Foundation of Ireland, Contract No.06/IN.1/I91 and conducted under the framework of the INSPIRE programme, funded by the Irish Government's Programme for Research in Third Level Institutions, Cycle 4, National Development Plan 2007-2013. O. Ualibek would like to thank the Government of Rep. of Kazakhstan under the Bolashak programme.

Supporting information

The transfer matrix approach developed in the manuscript can be easily used also to simulate the optical response measured with other spectroscopic techniques and can be utilised with different materials.

In this section the response of Ag NP arrays measured with RAS will be compared with simulations. RAS measures the difference in reflectance (Δr) at a normal incidence between two orthogonal directions in the surface plane (x, y) normalized to the mean reflectance (r):[56]

$$\frac{\Delta r}{r} = \frac{2(r_x - r_y)}{r_x + r_y}, \tag{8}$$

where r are the complex Fresnel reflection amplitudes. As before, the x and y indexes in Eq. (8) refer to the in-plane directions along and perpendicular to the array axes respectively. As for the complex ratio of SE, RAS can also be simulated using the same transfer matrix. During the simulations the incidence angle was considered to be close to normal incidence(3°) and the p and s components are made to coincide with the x and y ones from Eq. (8). The RAS system is a home built system which follows the 2 polarisers and photo-elastic modulator scheme.[57] The real and imaginary part of RAS has been measured immediately after exposure of the sample to atmosphere. A comparison with the theory are reproduced in Figure 8. Also in this case, the spectra appear well reproduced. The disagreement in the peak intensity is related to the non perfect matching between theory and experiment for the y resonance (appearing here as the negative peak). The origin of the real component

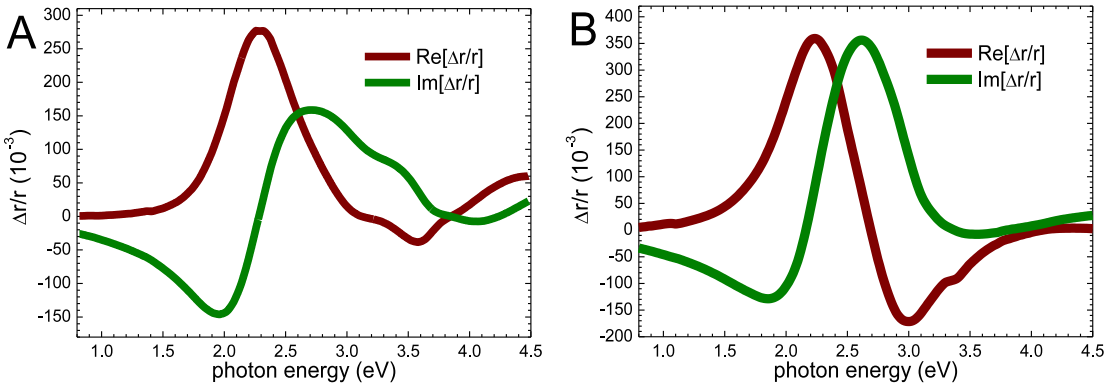

Figure 8: Experimental (A) and simulated (B) RAS spectra for the Ag NP arrays grown by glancing angle of incidence.

of the RAS signal measured has been recently studied in our group and it was found to coincide with the difference between an intense positive (x) and a less intense negative (y)

peak shifted towards higher energies.[45] For the system under study it is suggested that the two resonances are placed closer in the experiment if compared with the simulation (see for example Figure 3 D in the text). As the peaks partially overlap, once the difference between the two peaks is considered, the measured RAS peak positions appear shifted if compared with the simulated ones (the same effect happens in Figure 3 D). At the same time, once the difference is calculated, the relative intensity of the peaks changes. As the imaginary component of the RAS is related to the real part by Kramers-Kronig relationship, its intensity and position is modified in this case. Once again we would like to point out that, as for the SE results, the difference between experiment and theory is then related to a non perfect agreement between the real response of the plasmonic layer dielectric function and the simulated effective plamsonic layer dielectric function rather than errors in the transfer matrix approach used.

We also verified that the formalism here developed is also valid for different materials. As glancing angle deposition is independent on the deposited material,[46] Au NP arrays can also be produced and their response measured using SE (see Figure 9 A for a SEM image of the surface after deposition). The real part of the pseudo dielectric function as measured by SE in the configuration parallel and perpendicular to the array are shown in Figure 9 B and C for multiple incidence angles. The optical response shows clear differences if compared with Ag NPs. The main x resonance is placed further in the IR (1.77 eV) and higher energy features measured for the Ag case are screened now by strong and broad features related to interband transitions.[46] We have simulated also in this case the response using our matrix approach. The Au dielectric function was taken from literature[58] and the free electron response corrected in order to take into consideration the reduced dimensions of the NPs.[47,59] In order to simplify the discussion, the same morphological parameters as the one used for Ag NPs are used during this simulations. However, the trend for different deposition angles measured in the experiment coincides with the behaviour simulated with our approach.

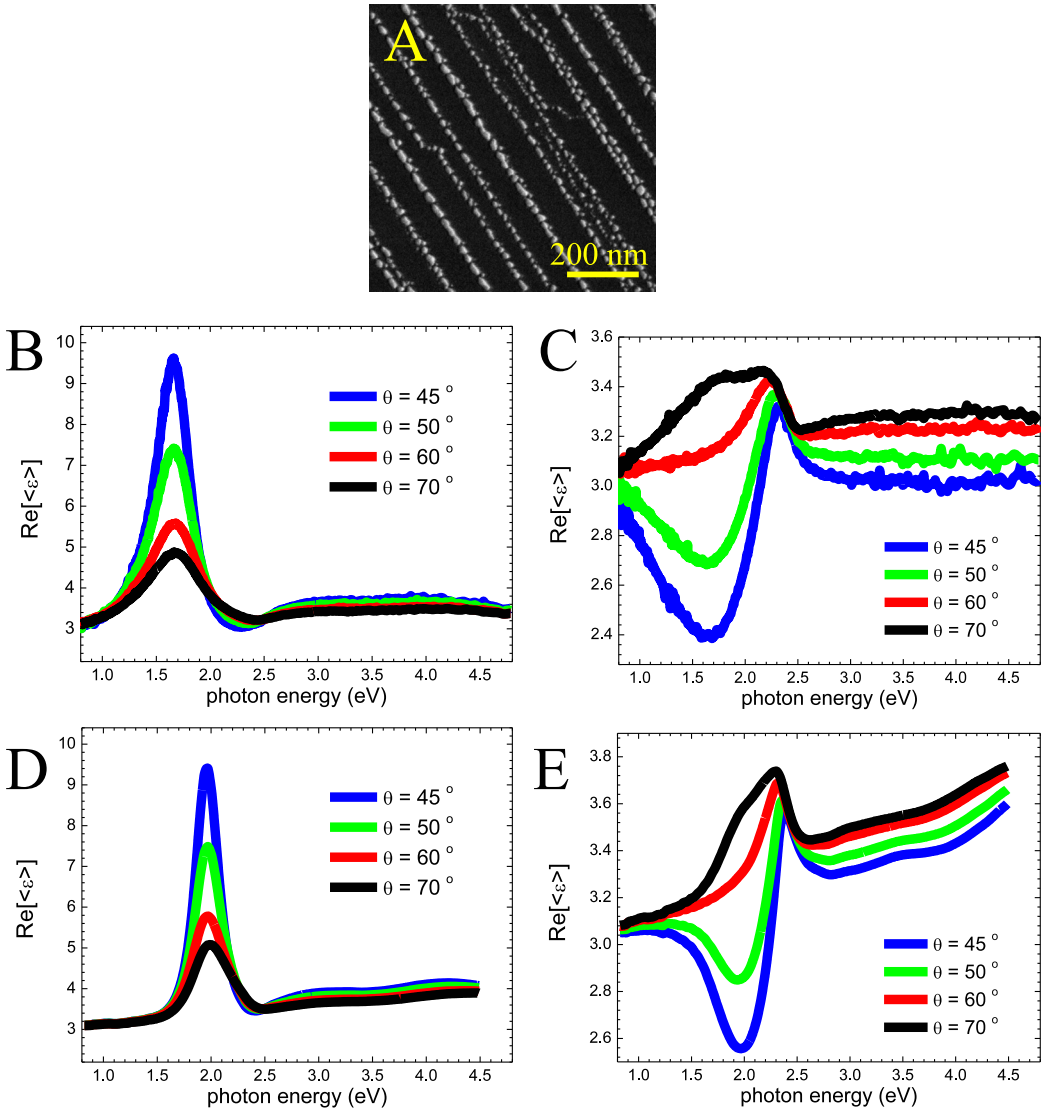

Figure 9: SE response of Au NP arrays. (A) SEM image of the in-plane morphology of the sample. Also gold NP arrays can be produced by glancing angle deposition. Measured pseudo dielectric function for the measurement configuration parallel (B) and perpendicular (C) to the array. The simulated behaviour for the two cases are shown in (C) and (D) respectively.

These results appear as a strong confirmation of the validity of the methodology utilised even when different materials are utilised and it is verified by comparison of the RAS results obtained from Ag NPs.

References

1. Kreibig, U.; Vollmer, M. *Optical Properties of Metal Clusters*; Springer, Berlin, 1957.

2. Brongersma, L.; Kik, P. *Surface Plasmon Nanophotonics*; Springer, Berlin, 2007.

3. Willets, K. A.; Van Duyne, R. P. Localized Surface Plasmon Resonance Spectroscopy and Sensing. *Annual Review of Physical Chemistry* **2007**, *58*, 267–297.

4. Homola, J. Surface Plasmon Resonance Sensors for Detection of Chemical and Biological Species. *Chemical Reviews* **2008**, *108*, 462–493, PMID: 18229953.

5. F., H. Symmetry Breaking in Plasmonic Nanocavities: Subradiant LSPR Sensing and a Tunable Fano Resonance. *Nano Lett.* **2008**, *8*, 3983.

6. N., V. Plasmon Line Shaping using Nanocrosses for High sensitivity LSPR Sensing. *Nano Lett.* **2011**, *11*, 391.

7. Nie, S.; Emory, S. R. Probing Single Molecules and Single Nanoparticles by Surface-Enhanced Raman Scattering. *Science* **1997**, *275*, 1102–1106.

8. Kim, S.; Jin, J.; Kim, Y.-J.; Park, I.-Y.; Kim, Y.; Kim, S.-W. High-harmonic generation by resonant plasmon field enhancement. *Nature* **2008**, *453*, 757–760.

9. Kinkhabwala, A.; Yu, Z.; Fan, S.; Avlasevich, Y.; Mullen, K.; E., M. Large single-molecule fluorescence enhancements produced by a bowtie nanoantenna. *Nature Phot.* **2009**, *3*, 654 – 657.

10. Atawer H.A., P. A. Plasmonics for improved photovoltaic devices. *Nat. Mater.* **2010**, *9*, 205–213.

11. Pala, R. A.; White, J.; Barnard, E.; Liu, J.; Brongersma, M. L. Design of Plasmonic Thin-Film Solar Cells with Broadband Absorption Enhancements. *Advanced Materials* **2009**, *21*, 3504–3509.

12. Munday, J. N.; Atwater, H. A. Large Integrated Absorption Enhancement in Plasmonic Solar Cells by Combining Metallic Gratings and Antireflection Coatings. *Nano Letters* **2011**, *11*, 2195–2201.

13. H., L.; E., C. The Optical Properties of Metal Nanoparticles: The Influence of Size, Shape, and Dielectric Environment. *Journal of Physical Chemistry B* **2003**, *107*, 668.

14. Gomez-Medina, R.; Yamamoto, N.; Nakano, M.; de Abajo, F. J. G. Mapping plasmons in nanoantennas via cathodoluminescence. *New Journal of Physics* **2008**, *10*, 105009.

15. Vesseur, E. J. R.; Garcia de Abajo, F. J.; Polman, A. Modal Decomposition of SurfaceâĹŠPlasmon Whispering Gallery Resonators. *Nano Letters* **2009**, *9*, 3147–3150, PMID: 19653636.

16. Scholl, J. A.; Koh, A. L.; Dionne, J. A. Quantum plasmon resonances of individual metallic nanoparticles. *Nature* **2012**, *483*, 421–427.

17. Nelayah, J.; Kociak, M.; Stephan, O.; Garcia de Abajo, F. J.; Tence, M.; Henrard, L.; Taverna, D.; Pastoriza-Santos, I.; Liz-Marzan, L. M.; Colliex, C. Mapping surface plasmons on a single metallic nanoparticle. *Nat. Phys.* **2007**, *3*, 348–353.

18. Azzam, R.; Bashara, N. *Ellipsometry and polarized light*; North Holland, 1977.

19. Losurdo, M.; Bergmair, M.; Bruno, G.; Cattelan, D.; Cobet, C.; de Martino, A.; Fleischer, K.; Dohcevic-Mitrovic, Z.; Esser, N.; Galliet, M. et al. Spectroscopic ellipsometry and polarimetry for materials and systems analysis at the nanometer scale: state-of-the-art, potential, and perspectives. *J. Nanopart. Res.* **2009**, *11*, 1521–1554.

20. Mok, K.; Du, N.; Schmidt, H. Vector-magneto-optical generalized ellipsometry. *Review of Scientific Instruments* **2011**, *82*, 033112.

21. Lo, Y.; Hsieh, W.; Chung, Y.; Tsai, S. An Approach for Measuring the Ellipsometric Parameters of Isotropic and Anisotropic Thin Films Using the Stokes Parameter Method. *J. Lightwave Technol.* **2012**, *30*, 2299–2306.

22. Wu, P. C.; Kim, T.-H.; Brown, A. S.; Losurdo, M.; Bruno, G.; Everitt, H. O. Real-time plasmon resonance tuning of liquid Ga nanoparticles by in situ spectroscopic ellipsometry. *Applied Physics Letters* **2007**, *90*, 103119.

23. Flores-Camacho, J. M.; Sun, L. D.; Saucedo-Zeni, N.; Weidlinger, G.; Hohage, M.; Zeppenfeld, P. Optical anisotropies of metal clusters supported on a birefringent substrate. *Phys. Rev. B* **2008**, *78*, 075416.

24. Wu, P. C.; Losurdo, M.; Kim, T.-H.; Garcia-Cueto, B.; Moreno, F.; Bruno, G.; Brown, A. S. GaâĂŞMg CoreâĂŞShell Nanosystem for a Novel Full Color Plasmonics. *The Journal of Physical Chemistry C* **2011**, *115*, 13571–13576.

25. Lodewijks, K.; Van Roy, W.; Borghs, G.; Lagae, L.; Van Dorpe, P. Boosting the Figure-Of-Merit of LSPR-Based Refractive Index Sensing by Phase-Sensitive Measurements. *Nano Letters* **2012**, *12*, 1655–1659.

26. Zhu, S.; Chen, T.; Liu, Y. C.; Liu, Y.; Yu, S. F. Influence of SiO2 Layer on the Dielectric Function of Gold Nanoparticles on Si Substrate **2012**, *15*, K5–K9.

27. Verre, R.; Fleischer, K.; Smith, C.; McAlinden, N.; McGilp, J. F.; Shvets, I. V. Probing the out-of-plane optical response of plasmonic nanostructures using spectroscopic ellipsometry. *Phys. Rev. B* **2011**, *84*, 085440.

28. Kelly, M.; Zollner, S.; Cardona, M. Modelling the optical response of surfaces measured

460 by spectroscopic ellipsometry: application to Si and Ge. *Surface Science* **1993**, *285*, 282
461 – 294.

462 29. Yamaguchi, T.; Yoshida, S.; Kinbara, A. Anomalous optical absorption of aggregated
463 silver films. *Thin Solid Films* **1973**, *18*, 63 – 70.

464 30. Yamaguchi, T.; Yoshida, S.; Kinbara, A. Optical effect of the substrate on the anomalous
465 absorption of aggregated silver films. *Thin Solid Films* **1974**, *21*, 173 – 187.

466 31. Valamanesh, M.; Borensztein, Y.; Langlois, C.; Lacaze, E. Substrate Effect on the Plas-
467 mon Resonance of Supported Flat Silver Nanoparticles. *J. Chem. Phys. C* **2011**, *115*,
468 2914–2922.

469 32. Fan, J. A.; Wu, C.; Bao, K.; Bao, J.; Bardhan, R.; Halas, N. J.; Manoharan, V. N.;
470 Nordlander, P.; Shvets, G.; Capasso, F. Self-Assembled Plasmonic Nanoparticle Clusters.
471 *Science* **2010**, *328*, 1135–1138.

472 33. Woo, K. C.; Shao, L.; Chen, H.; Liang, Y.; Wang, J.; Lin, H. Universal Scaling and
473 Fano Resonance in the Plasmon Coupling between Gold Nanorods. *ACS Nano* **2011**, *5*,
474 5976–5986.

475 34. F., H. Tunability of Subradiant Dipolar and Fano-Type Plasmon Resonances in Metallic
476 Ring/Disk Cavities: Implications for Nanoscale Optical Sensing. *ACS Nano* **2009**, *3*,
477 643.

478 35. Svedendahl, M.; KÃdll, M. Fano Interference between Localized Plasmons and Interface
479 Reflections. *ACS Nano* **2012**, *6*, 7533–7539.

480 36. Sanchez-Iglesias, A.; Grzelczak, M.; Rodrguez-Gonzlez, B.; A. lvarez Puebla, R.; Liz-
481 Marzan, L. M.; A. Kotov, N. Gold Colloids with Unconventional Angled Shapes. *Lang-*
482 *muir* **2009**, *25*, 11431.

37. Nelayah, J.; Kociak, M.; Stephan, O.; Geuquet, N.; Henrard, L.; Garcia de Abajo, F. J.; Pastoriza-Santos, I.; Liz-Marzan, L. M.; Colliex, C. Two-Dimensional Quasistatic Stationary Short Range Surface Plasmons in Flat Nanoprisms. *Nano Letters* **2010**, *10*, 902–907, PMID: 20163134.

38. Kumar, P. S.; Pastoriza-Santos, I.; RodrÃŋguez-GonzÃąlez, B.; de Abajo, F. J. G.; Liz-MarzÃąn, L. M. High-yield synthesis and optical response of gold nanostars. *Nanotechnology* **2008**, *19*, 015606.

39. Oubre, C.; Nordlander, P. Optical Properties of Metallodielectric Nanostructures Calculated Using the Finite Difference Time Domain Method. *The Journal of Physical Chemistry B* **2004**, *108*, 17740–17747.

40. Draine, B. T.; Flatau, P. J. Discrete-dipole approximation for scattering calculations. *J. Opt. Soc. Am. A* **1994**, *11*, 1491–1499.

41. Charles, D. E.; Aherne, D.; Gara, M.; Ledwith, D. M.; Gunko, Y. K.; Kelly, J. M.; Blau, W. J.; Brennan-Fournet, M. E. Versatile Solution Phase Triangular Silver Nanoplates for Highly Sensitive Plasmon Resonance Sensing. *ACS Nano* **2010**, *4*, 55–64, PMID: 20030362.

42. Sugawara, A.; Hembree, G.; Scheinfein, M. R. Self-organized mesoscopic magnetic structures. *Journal of Applied Physics* **1997**, *82*, 5662.

43. Oates, T.; Keller, A.; Facsko, S.; Mï£¡cklich, A. Aligned Silver Nanoparticles on Rippled Silicon Templates Exhibiting Anisotropic Plasmon Absorption. *Plasmonics* **2007**, *2*, 47.

44. Cuccureddu, F.; Murphy, S.; Shvets, I.; Porcu, M.; Zandbergen, H. W. Plasmon Resonance in Silver Nanoparticles Arrays Grown by Atomic Terrace Low-Angle Shadowing. *Nano letters* **2008**, *8*, 3248.

45. Verre, R.; Fleischer, K.; Sofin, R. G. S.; McAlinden, N.; McGilp, J. F.; Shvets, I. V. In situ characterization of one-dimensional plasmonic Ag nanocluster arrays. *Phys. Rev. B* **2011**, *83*, 125432–125440.

46. Verre, R.; Fleischer, K.; Ualibek, O.; Shvets, I. V. Self-assembled broadband plasmonic nanoparticle arrays for sensing applications. *Applied Physics Letters* **2012**, *100*, 031102.

47. Verre, R.; Fleischer, K.; McGilp, J. F.; Fox, D.; Behan, G.; Zhang, H.; Shvets, I. V. Controlled in situ growth of tunable plasmonic self-assembled nanoparticle arrays. *Nanotechnology* **2012**, *23*, 035606.

48. Plieth, W.; Naegele, K. Lieber die bestimmung der optischen konstanten dnster oberflchenschichten und das problem der schichtdicke. *Surf. Sci.* **1977**, *64*, 484 – 496.

49. Santos, P. V.; Koopmans, B.; Esser, N.; Schmidt, W. G.; Bechstedt, F. Optical Properties of Ordered As Layers on InP(110) Surfaces. *Phys. Rev. Lett.* **1996**, *77*, 759–762.

50. Schubert, M. Polarization-dependent optical parameters of arbitrarily anisotropic homogeneous layered systems. *Phys. Rev. B* **1996**, *53*, 4265–4274.

51. Schubert, M.; Tiwald, T. E.; Woollam, J. A. Explicit Solutions for the Optical Properties of Arbitrary Magneto-Optic Materials in Generalized Ellipsometry. *Appl. Opt.* **1999**, *38*, 177–187.

52. Bohren, C.; Huffman, D. *Absorption and scattering of light by small particles*; Wiley, New York, 1983.

53. Abe, M.; Suwa, T. Surface plasma resonance and magneto-optical enhancement in composites containing multicore-shell structured nanoparticles. *Phys. Rev. B* **2004**, *70*, 235103.

54. Heffelfinger, J. R.; Bench, M. W.; Carter, C. B. Steps and the structure of the (0001) α -alumina surface. *Surface Science* **1997**, *370*, 168.

530 55. Verre, R.; Sofin, R.; Usov, V.; Fleischer, K.; Fox, D.; Behan, G.; Zhang, H.; Shvets, I.
531 Equilibrium faceting formation in vicinal Al2O3 (0001) surface caused by annealing.
532 *Surface Science* **2012**, *606*, 1815 – 1820.

533 56. Weightman, P.; Martin, D. S.; Cole, R. J.; Farrell, T. Reflection anisotropy spectroscopy.
534 *Reports of Progress in Physics* **2005**, *68*, 1251.

535 57. D.E.Aspnes, Above-bandgap optical anisotropies in cubic semiconductors: A visible-near
536 ultraviolet probe of surfaces. *J. Vac. Sci. Technol. B* **1985**, *3*, year.

537 58. Johnson, P. B.; Christy, R. W. Optical Constants of the Noble Metals. *Phys. Rev. B*
538 **1972**, *6*, 4370–4379.

539 59. Hövel, H.; Fritz, S.; Hilger, A.; Kreibig, U.; Vollmer, M. Width of cluster plasmon
540 resonances: Bulk dielectric functions and chemical interface damping. *Phys. Rev. B*
541 **1993**, *48*, 18178–18188.